



# Dissimilar nonhomogeneous magneto-electroelastic layers with moving crack at the interface

Mojtaba Ayatollahi · Amir G. Milan

Received: 30 March 2021 / Accepted: 29 January 2022 / Published online: 13 March 2022  
© The Author(s), under exclusive licence to Springer Nature B.V. 2022

**Abstract** In this paper, the dynamic fracture problem of multiple moving cracks at the interface of two dissimilar functionally graded magneto-electroelastic (FGMEE) layers subjected to anti-plane mechanical and in-plane magneto-electrical loads is considered. The magneto-electromechanical properties are assumed to vary exponentially with the coordinate perpendicular to the cracks. The integral transform technique is employed to solve the moving crack problem at the interface of dissimilar FGMEE layers. Numerical values for the field intensity factors are graphically presented and the effects of the crack velocity, nonhomogeneity parameter, and material volume fraction on the field intensity factor are examined.

**Keywords** Distributed dislocation technique · Field intensity factors · Functionally graded material · Magneto-electroelastic layer · Moving cracks

## 1 Introduction

In practical applications, the composite materials that consist of piezoelectric and piezomagnetic phases seem to have certain reliability problems arising largely from high stresses, poor interfacial bonding strength, and low toughness. To improve their application and reliability, FGMs can be extended to piezoelectric/piezomagnetic and magneto-electroelastic materials.

Functionally graded materials (FGMs) are essentially inhomogeneous composites, which have characteristics of spatially varying material properties to enhance the bonding strength. In designing components involving FGMs, it is important to consider imperfections, such as cracks, which are often pre-existed as those generated by external loads during service. Fracture mechanics of FGMs plays an important role in the analysis and design of many complex smart structures and devices.

This study was directed at the dynamic fracture mechanics of such materials when there are multiple moving cracks at the interface and sought to find parameters that govern the crack growth such as the crack stress intensity factors and energy release rate.

Numerous publications have addressed the moving crack problem in a piezoelectric solid (see, for example, the works of [1]–[4]). Gao et al. [5] solved a generalized 2D problem of an electrically permeable interface crack

---

M. Ayatollahi (✉) · A. G. Milan  
Faculty of Engineering, University of Zanjan, P.O. Box 45195-313, Zanjan, Iran  
e-mail: mo\_ayatollahi@znu.ac.ir

between two dissimilar MEE solids under general loading. Gao and Noda [6] studied the problem of an interface crack between two dissimilar magneto-electroelastic materials under uniform heat flow. The problem of a Griffith moving crack in an MEE material with a permeable condition was analyzed by Hu and Li [7]. The problem of moving crack at the interface of two dissimilar MEE materials under shear and in-plane electric and magnetic loads was analyzed by Hu et al. [8]. They obtained the closed-form expressions for field intensity factors.

Several studies have been performed for the dynamic anti-plane behavior of two dissimilar magneto-electroelastic materials involving an anti-plane shear interfacial moving crack; see, e.g., the works of [9–13, 15, 20, 21].

The propagation of an interface Griffith crack between two dissimilar FGPM layers under anti-plane shear was analyzed by Shin and Lee [14]. In this study, The Fourier transformation is employed to solve the Volterra dislocation in a functionally graded MEE half-plane. Fu et al. [16] solved the problem of a moving crack in a functionally graded MEE strip under anti-plane mechanical and in-plane electric and magnetic loadings. Hu and Chen [17] have addressed the problem of moving crack in an MEE material under in-plane mechanical, electric, and magnetic loading. In another paper, Hu and Chen [18] investigated the interface crack moving between MEE and functionally elastic layers. Yue and Wan [19] discussed the problem of periodic mode-III Yoffe-type cracks propagating subsonically along with the interfaces in a multilayered piezomagnetic/piezoelectric composite under in-plane magnetic or electric field. The problem of several moving cracks in a functionally graded magneto-electroelastic strip subjected to anti-plane mechanical and in-plane electric and magnetic loading is solved by Bagheri et al. [4]. Ma et al. [23] studied the plane-strain problem of a moving crack at the interface of two dissimilar MEE materials. Ayatollahi et al. [24] investigated the dynamic fracture behavior of a functionally graded magneto-electroelastic half-plane containing multiple moving cracks under different electric and magnetic boundary conditions. Bagheri and Noroozi [25] employed the distributed dislocation technique to analyze a piezoelectric half-plane containing several moving cracks under in-plane electro-elastic loading.

The technique developed in this study is useful for the dynamic fracture mechanics studies of two bonded MEE layers with any number of cracks at the interface. The problem is solved for various values of the nonhomogeneity parameter and different values of loading parameters. This paper is organized as follows. The mathematical formulation of the problem is given in Sect. 2. Section 3 deals with the constructions of the integral equations for two bonded FGME layers weakened by several moving interface cracks. The numerical results are then presented and discussed in Sect. 4. Finally, concluding remarks are given in Sect. 5.

## 2 Mathematical Formulation of the Problem

The usefulness of distributed dislocation technique in generating solutions to multiple crack problems has been well demonstrated in the literature for the static case. In this section, we describe the layered intelligent structures composed of two bonded dissimilar FGME layers weakened by moving dislocation. Both materials are nonhomogeneous with an exponential property variation in the  $y$ -direction. In this case, if there is no body force and electric charge density and magnetocharge density, the constitutive equations for the FGME material can be written as

$$\begin{pmatrix} \sigma_{ZY}^{(k)}(X, Y, t) \\ D_Y^{(k)}(X, Y, t) \\ B_Y^{(k)}(X, Y, t) \end{pmatrix} = \begin{pmatrix} c_{44}^{(k)}(Y) & e_{15}^{(k)}(Y) & h_{15}^{(k)}(Y) \\ e_{15}^{(k)}(Y) & -d_{11}^{(k)}(Y) & -\beta_{11}^{(k)}(Y) \\ h_{15}^{(k)}(Y) & -\beta_{11}^{(k)}(Y) & -\gamma_{11}^{(k)}(Y) \end{pmatrix} \begin{pmatrix} \partial W^{(k)}/\partial Y \\ \partial \varphi^{(k)}/\partial Y \\ \partial \psi^{(k)}/\partial Y \end{pmatrix},$$

$$\begin{pmatrix} \sigma_{ZX}^{(k)}(X, Y, t) \\ D_X^{(k)}(X, Y, t) \\ B_X^{(k)}(X, Y, t) \end{pmatrix} = \begin{pmatrix} c_{44}^{(k)}(Y) & e_{15}^{(k)}(Y) & h_{15}^{(k)}(Y) \\ e_{15}^{(k)}(Y) & -d_{11}^{(k)}(Y) & -\beta_{11}^{(k)}(Y) \\ h_{15}^{(k)}(Y) & -\beta_{11}^{(k)}(Y) & -\gamma_{11}^{(k)}(Y) \end{pmatrix} \begin{pmatrix} \partial W^{(k)}/\partial X \\ \partial \varphi^{(k)}/\partial X \\ \partial \psi^{(k)}/\partial X \end{pmatrix}, \quad k = 1, 2, \quad (1)$$

where  $\sigma_{ZY}$ ,  $\sigma_{ZX}$ ,  $D_X$ ,  $D_Y$  and  $B_X$ ,  $B_Y$  are the component of stress, electric displacement, and magnetic induction, respectively;  $c_{44}^{(k)}$ ,  $e_{15}^{(k)}$ ,  $h_{15}^{(k)}$  and  $\beta_{11}^{(k)}$ , denote the elastic, piezoelectric, piezomagnetic, and electromagnetic constants;  $d_{11}^{(k)}$ , and  $\gamma_{11}^{(k)}$ , are dielectric permeability and magnetopermeability. Note that the layer number will be designed by a superscript  $k = 1, 2$ . The nontrivial ones of the equations of motion and Maxwell's equations for

magneto-electroelastic materials take the following forms:

$$\begin{aligned} \frac{\partial \sigma_{ZX}^{(k)}(X, Y, t)}{\partial X} + \frac{\partial \sigma_{ZY}^{(k)}(X, Y, t)}{\partial Y} &= \rho^{(k)} \frac{\partial^2 W^{(k)}(X, Y, t)}{\partial t^2}, \\ \frac{\partial D_X^{(k)}(X, Y, t)}{\partial X} + \frac{\partial D_Y^{(k)}(X, Y, t)}{\partial Y} &= 0, \\ \frac{\partial B_X^{(k)}(X, Y, t)}{\partial X} + \frac{\partial B_Y^{(k)}(X, Y, t)}{\partial Y} &= 0, \quad k = 1, 2. \end{aligned} \tag{2}$$

To make the analysis tractable, the material possesses the following inhomogeneous properties:

$$\begin{aligned} c_{44}^{(1)} &= c_{440} \exp(2\beta Y), \quad e_{15}^{(1)} = e_{150} \exp(2\beta Y), \quad h_{15}^{(1)} = h_{150} \exp(2\beta Y), \quad \rho^{(1)} = \rho_0 \exp(2\beta Y), \\ \beta_{11}^{(1)} &= \beta_{110} \exp(2\beta Y), \quad d_{11}^{(1)} = d_{110} \exp(2\beta Y), \quad \gamma_{11}^{(1)} = \gamma_{110} \exp(2\beta Y) \quad 0 < Y < h_1, \\ c_{44}^{(2)} &= c_{440} \exp(2\lambda Y), \quad e_{15}^{(2)} = e_{150} \exp(2\lambda Y), \quad h_{15}^{(2)} = h_{150} \exp(2\lambda Y), \quad \rho^{(2)} = \rho_0 \exp(2\lambda Y), \\ \beta_{11}^{(2)} &= \beta_{110} \exp(2\lambda Y), \quad d_{11}^{(2)} = d_{110} \exp(2\lambda Y), \quad \gamma_{11}^{(2)} = \gamma_{110} \exp(2\lambda Y), \quad -h_2 < Y < 0, \end{aligned} \tag{3}$$

where  $\beta$  and  $\lambda$  are the gradient of material properties and are positive or negative constants. This model includes the effects of varying material constants and mass density but ignores the effect of the spatial variation of wave speed. Substituting from (3) and (1) into the governing equation (2), we obtain

$$\begin{aligned} c_{440} \nabla^2 W^{(1)} + e_{150} \nabla^2 \varphi^{(1)} + h_{150} \nabla^2 \psi^{(1)} + 2\beta c_{440} \frac{\partial W^{(1)}}{\partial Y} + 2\beta e_{150} \frac{\partial \varphi^{(1)}}{\partial Y} + 2\beta h_{150} \frac{\partial \psi^{(1)}}{\partial Y} &= \rho_0 \frac{\partial^2 W^{(1)}}{\partial t^2}, \\ e_{150} \nabla^2 W^{(1)} - d_{110} \nabla^2 \varphi^{(1)} - \beta_{110} \nabla^2 \psi^{(1)} + 2\beta e_{150} \frac{\partial W^{(1)}}{\partial Y} - 2\beta d_{110} \frac{\partial \varphi^{(1)}}{\partial Y} - 2\beta \beta_{110} \frac{\partial \psi^{(1)}}{\partial Y} &= 0, \\ h_{150} \nabla^2 W^{(1)} - \beta_{110} \nabla^2 \varphi^{(1)} - \gamma_{110} \nabla^2 \psi^{(1)} + 2\beta h_{150} \frac{\partial W^{(1)}}{\partial Y} - 2\beta \beta_{110} \frac{\partial \varphi^{(1)}}{\partial Y} - 2\beta \gamma_{110} \frac{\partial \psi^{(1)}}{\partial Y} &= 0, \quad 0 < Y < h_1, \\ c_{440} \nabla^2 W^{(2)} + e_{150} \nabla^2 \varphi^{(2)} + h_{150} \nabla^2 \psi^{(2)} + 2\lambda c_{440} \frac{\partial W^{(2)}}{\partial Y} + 2\lambda e_{150} \frac{\partial \varphi^{(2)}}{\partial Y} + 2\lambda h_{150} \frac{\partial \psi^{(2)}}{\partial Y} &= \rho_0 \frac{\partial^2 W^{(2)}}{\partial t^2}, \\ e_{150} \nabla^2 W^{(2)} - d_{110} \nabla^2 \varphi^{(2)} - \beta_{110} \nabla^2 \psi^{(2)} + 2\lambda e_{150} \frac{\partial W^{(2)}}{\partial Y} - 2\lambda d_{110} \frac{\partial \varphi^{(2)}}{\partial Y} - 2\lambda \beta_{110} \frac{\partial \psi^{(2)}}{\partial Y} &= 0, \\ h_{150} \nabla^2 W^{(2)} - \beta_{110} \nabla^2 \varphi^{(2)} - \gamma_{110} \nabla^2 \psi^{(2)} + 2\lambda h_{150} \frac{\partial W^{(2)}}{\partial Y} - 2\lambda \beta_{110} \frac{\partial \varphi^{(2)}}{\partial Y} - 2\lambda \gamma_{110} \frac{\partial \psi^{(2)}}{\partial Y} &= 0, \quad -h_2 < Y < 0, \end{aligned} \tag{4}$$

where  $\nabla^2 = \partial^2/\partial X^2 + \partial^2/\partial Y^2$  is the two-dimensional Laplacian operator. By introducing two new auxiliary functions  $\bar{\varphi}^{(k)}$  and  $\bar{\psi}^{(k)}$   $k = 1, 2$  such that ([7]).

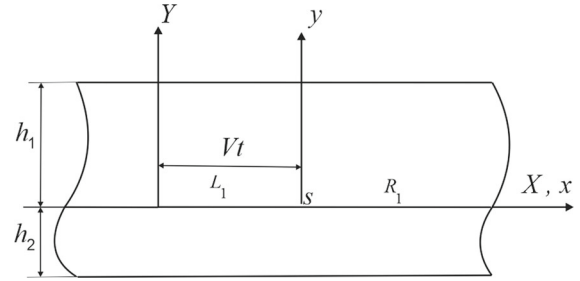
$$\begin{aligned} \varphi^{(k)}(X, Y, t) &= \bar{\varphi}^{(k)}(X, Y, t) - m W^{(k)}(X, Y, t), \\ \psi^{(k)}(X, Y, t) &= \bar{\psi}^{(k)}(X, Y, t) - n W^{(k)}(X, Y, t), \end{aligned} \tag{5}$$

where  $m = (\beta_{110}h_{150} - \gamma_{110}e_{150})/(d_{110}\gamma_{110} - (\beta_{110})^2)$ ,  $n = (\beta_{110}e_{150} - d_{110}h_{150})/(d_{110}\gamma_{110} - (\beta_{110})^2)$  are the known constants. Substituting (5) into (4), we can obtain the governing equation as follows:

$$\begin{aligned} \nabla^2 W^{(k)} + 2\xi \frac{\partial W^{(k)}}{\partial Y} &= \frac{\rho_0}{\tilde{c}_{44}} \frac{\partial^2 W^{(k)}}{\partial t^2}, \\ \nabla^2 \bar{\varphi}^{(k)} + 2\xi \frac{\partial \bar{\varphi}^{(k)}}{\partial Y} &= 0, \\ \nabla^2 \bar{\psi}^{(k)} + 2\xi \frac{\partial \bar{\psi}^{(k)}}{\partial Y} &= 0, \quad \xi \in \{\beta, \lambda\}, \end{aligned} \tag{6}$$

where  $\tilde{c}_{44} = c_{440} - e_{150}m - h_{150}n$  is the magneto-electroelastic stiffened constant. For the analysis of moving interfacial cracks, however, the solution to moving screw dislocation at the interface is required. To this end,

**Fig. 1** Schematic view of moving dislocation at the interface of dissimilar magneto-electroelastic layers



consider a screw dislocation moving with constant velocity  $V$ , along the  $X$ -direction, it is convenient to introduce a new coordinate system  $oxyz$  that moves at the same speed as the moving dislocation (Fig. 1). The relation between the initial coordinate system and moving coordinate system is defined by

$$x = X - Vt, \quad y = Y, \quad z = Z. \tag{7}$$

Equation (5) becomes independent of  $t$  and reduces to the following equation in the new coordinate system

$$\begin{aligned} K^2 \frac{\partial^2 w^{(k)}}{\partial x^2} + \frac{\partial^2 w^{(k)}}{\partial y^2} + 2\xi \frac{\partial w^{(k)}}{\partial y} &= 0, \\ \nabla^2 \bar{\varphi}^{(k)} + 2\xi \frac{\partial \bar{\varphi}^{(k)}}{\partial y} &= 0, \\ \nabla^2 \bar{\psi}^{(k)} + 2\xi \frac{\partial \bar{\psi}^{(k)}}{\partial y} &= 0, \quad k = 1, 2, \end{aligned} \tag{8}$$

where  $K = \sqrt{1 - (V/C)^2}$  and  $C = \sqrt{\tilde{c}_{44}/\rho_0}$ . The basic equation (1) can be expressed as follows:

$$\begin{aligned} \sigma_{zy}^{(k)}(x, y) &= \left( \tilde{c}_{44} \frac{\partial w^{(k)}}{\partial y} + e_{150} \frac{\partial \bar{\varphi}^{(k)}}{\partial y} + h_{150} \frac{\partial \bar{\psi}^{(k)}}{\partial y} \right) e^{2\xi y}, \\ D_y^{(k)}(x, y) &= - \left( d_{110} \frac{\partial \bar{\varphi}^{(k)}}{\partial y} + \beta_{110} \frac{\partial \bar{\psi}^{(k)}}{\partial y} \right) e^{2\xi y}, \\ B_y^{(k)}(x, y) &= - \left( \beta_{110} \frac{\partial \bar{\varphi}^{(k)}}{\partial y} + \gamma_{110} \frac{\partial \bar{\psi}^{(k)}}{\partial y} \right) e^{2\xi y}, \quad k = 1, 2. \end{aligned} \tag{9}$$

A single magneto-electroelastic dislocation is located at the origin. The conditions representing the magneto-electroelastic screw dislocation together with the jump in the electric and magnetic potentials may be expressed as

$$\begin{aligned} w^{(1)}(x, 0^+) - w^{(2)}(x, 0^-) &= b_z H(x), \\ \varphi^{(1)}(x, 0^+) - \varphi^{(2)}(x, 0^-) &= b_\varphi H(x), \\ \psi^{(1)}(x, 0^+) - \psi^{(2)}(x, 0^-) &= b_\psi H(x), \end{aligned} \tag{10}$$

where  $H(\cdot)$  is the Heaviside step function. In Eq. (10),  $b_z$ ,  $b_\varphi$  and  $b_\psi$  are the dislocation Burgers vectors of generalized magneto-electroelastic dislocation. The traction and charges-free conditions on the layer's boundaries can be written down in the following form:

$$\begin{aligned} \sigma_{zy}^{(1)}(x, h_1) = \sigma_{zy}^{(2)}(x, -h_2) &= 0, \\ D_y^{(1)}(x, h_1) = D_y^{(2)}(x, -h_2) &= 0, \\ B_y^{(1)}(x, h_1) = B_y^{(2)}(x, -h_2) &= 0. \end{aligned} \tag{11}$$

Also, the continuity conditions  $y = 0$  can be written as

$$\begin{aligned}
 \sigma_{zy}^{(1)}(x, 0^+) &= \sigma_{zy}^{(2)}(x, 0^-), \\
 D_y^{(1)}(x, 0^+) &= D_y^{(2)}(x, 0^-), \\
 B_y^{(1)}(x, 0^+) &= B_y^{(2)}(x, 0^-).
 \end{aligned}
 \tag{12}$$

By solving Eq. (8) and taking the inverse Fourier transform, we find that

$$\begin{aligned}
 w^{(1)}(x, y) &= \frac{e^{-\beta y}}{2\pi} \int_{-\infty}^{+\infty} (A_1^{(1)}(\omega)e^{-\gamma_1 y} + A_2^{(1)}(\omega)e^{\gamma_1 y})e^{i\omega x} d\omega, \\
 \bar{\varphi}^{(1)}(x, y) &= \frac{e^{-\beta y}}{2\pi} \int_{-\infty}^{+\infty} (B_1^{(1)}(\omega)e^{-\gamma_2 y} + B_2^{(1)}(\omega)e^{\gamma_2 y})e^{i\omega x} d\omega, \\
 \bar{\psi}^{(1)}(x, y) &= \frac{e^{-\beta y}}{2\pi} \int_{-\infty}^{+\infty} (C_1^{(1)}(\omega)e^{-\gamma_2 y} + C_2^{(1)}(\omega)e^{\gamma_2 y})e^{i\omega x} d\omega,
 \end{aligned}
 \tag{13a}$$

and

$$\begin{aligned}
 w^{(2)}(x, y) &= \frac{e^{-\lambda y}}{2\pi} \int_{-\infty}^{+\infty} (A_1^{(2)}(\omega)e^{-\gamma_3 y} + A_2^{(2)}(\omega)e^{\gamma_3 y})e^{i\omega x} d\omega, \\
 \bar{\varphi}^{(2)}(x, y) &= \frac{e^{-\lambda y}}{2\pi} \int_{-\infty}^{+\infty} (B_1^{(2)}(\omega)e^{-\gamma_4 y} + B_2^{(2)}(\omega)e^{\gamma_4 y})e^{i\omega x} d\omega, \\
 \bar{\psi}^{(2)}(x, y) &= \frac{e^{-\lambda y}}{2\pi} \int_{-\infty}^{+\infty} (C_1^{(2)}(\omega)e^{-\gamma_4 y} + C_2^{(2)}(\omega)e^{\gamma_4 y})e^{i\omega x} d\omega,
 \end{aligned}
 \tag{13b}$$

where  $\gamma_1 = \sqrt{\beta^2 + (K\omega)^2}$ ,  $\gamma_2 = \sqrt{\beta^2 + \omega^2}$ ,  $\gamma_3 = \sqrt{\lambda^2 + (K\omega)^2}$  and  $\gamma_4 = \sqrt{\lambda^2 + \omega^2}$ . This completes the formulation of the problem for the bonded dissimilar FGME layers in which the functions  $A_i^{(2)}$ ,  $B_i^{(2)}$  and  $C_i^{(2)}$ ,  $i \in \{1, 2\}$  are determined from the boundary conditions. A simple calculation leads to the stress, electric displacement, and magnetic induction expressions at the lower layer that are found to be

$$\begin{aligned}
 \sigma_{zy}^{(2)}(x, y) &= -\frac{\tilde{c}_{44}b_z e^{\lambda y}}{2\pi} \int_{-\infty}^{+\infty} e^{\gamma_3 y} (1 - e^{-2\gamma_3(h_2+y)}) \frac{(\lambda - \gamma_3)}{P\hat{R} - \hat{P}} (\pi\delta(\omega) - i/\omega) e^{i\omega x} d\omega \\
 &\quad - \frac{(e_{150}m + h_{150}n)b_z e^{\lambda y}}{2\pi} \int_{-\infty}^{+\infty} e^{\gamma_4 y} (1 - e^{-2\gamma_4(h_2+y)}) \frac{(\lambda - \gamma_4)}{\hat{Q} - QR} (\pi\delta(\omega) - i/\omega) e^{i\omega x} d\omega \\
 &\quad + \frac{(e_{150}b_\varphi + h_{150}b_\psi)e^{\lambda y}}{2\pi} \int_{-\infty}^{+\infty} e^{\gamma_4 y} (1 - e^{-2\gamma_4(h_2+y)}) \frac{(\lambda - \gamma_4)}{\hat{Q} - QR} (\pi\delta(\omega) - i/\omega) e^{i\omega x} d\omega, \\
 D_y^{(2)}(x, y) &= \frac{(d_{110}m + \beta_{110}n)b_z e^{\lambda y}}{2\pi} \int_{-\infty}^{+\infty} e^{\gamma_4 y} (1 - e^{-2\gamma_4(h_2+y)}) \frac{(\lambda - \gamma_4)}{\hat{Q} - QR} (\pi\delta(\omega) - i/\omega) e^{i\omega x} d\omega \\
 &\quad - \frac{(d_{110}b_\varphi + \beta_{110}b_\psi)e^{\lambda y}}{2\pi} \int_{-\infty}^{+\infty} e^{\gamma_4 y} (1 - e^{-2\gamma_4(h_2+y)}) \frac{(\lambda - \gamma_4)}{\hat{Q} - QR} (\pi\delta(\omega) - i/\omega) e^{i\omega x} d\omega,
 \end{aligned}$$

$$\begin{aligned}
 B_y^{(2)}(x, y) = & \frac{(\beta_{110}m + \gamma_{110}n)b_z e^{\lambda y}}{2\pi} \int_{-\infty}^{+\infty} e^{\gamma_4 y} (1 - e^{-2\gamma_4(h_2+y)}) \frac{(\lambda - \gamma_4)}{\hat{Q} - QR} (\pi \delta(\omega) - i/\omega) e^{i\omega x} d\omega \\
 & - \frac{(\beta_{110}b_\phi + \gamma_{110}b_\psi) e^{\lambda y}}{2\pi} \int_{-\infty}^{+\infty} e^{\gamma_4 y} (1 - e^{-2\gamma_4(h_2+y)}) \frac{(\lambda - \gamma_4)}{\hat{Q} - QR} (\pi \delta(\omega) - i/\omega) e^{i\omega x} d\omega. \tag{14}
 \end{aligned}$$

To evaluate the stress components numerically, the integrals in Eq. (14) should be split into odd and even parts to arrive at

$$\begin{aligned}
 \sigma_{zy}^{(2)}(x, y) = & -\frac{\tilde{c}_{44}b_z e^{\lambda y}}{\pi} T_1(\gamma_1, \gamma_3) - \frac{e^{\lambda y}}{\pi} [(e_{150}m + h_{150}n)b_z - e_{150}b_\phi - h_{150}b_\psi] T_2(\gamma_2, \gamma_4), \\
 D_y^{(2)}(x, y) = & \frac{e^{\lambda y}}{\pi} [(d_{110}m + \beta_{110}n)b_z - d_{110}b_\phi - \beta_{110}b_\psi] T_2(\gamma_2, \gamma_4), \\
 B_y^{(2)}(x, y) = & \frac{e^{\lambda y}}{\pi} [(\beta_{110}m + \gamma_{110}n)b_z - \beta_{110}b_\phi - \gamma_{110}b_\psi] T_2(\gamma_2, \gamma_4). \tag{15}
 \end{aligned}$$

The expressions for  $T_1(\gamma_1, \gamma_3)$  and  $T_2(\gamma_2, \gamma_4)$  are given in Appendix A. The field components in Eq. (15) are unbounded for points in the vicinity of dislocation. To investigate and to separate the possible singular part of the singular parts of the stress component, electric displacement, and magnetic induction in (15), the asymptotic behavior of the inner integral must be examined. Thus, to identify the type of singularity, we carry out the asymptotic analysis of the improper integrals by observing that for large values of  $\omega \rightarrow \infty$ , from (15), we obtain

$$\begin{aligned}
 \sigma_{zy}^{(2)}(x, y) = & -\frac{\tilde{c}_{44}Kb_z e^{\lambda y}}{2\pi} \frac{x}{x^2 + (Ky)^2} - \frac{e^{\lambda y} [(e_{150}m + h_{150}n)b_z - e_{150}b_\phi - h_{150}b_\psi]}{2\pi} \frac{x}{x^2 + y^2} \\
 & - \frac{\tilde{c}_{44}b_z e^{\lambda y}}{\pi} T_3(\gamma_1, \gamma_3) - \frac{e^{\lambda y} [(e_{150}m + h_{150}n)b_z - e_{150}b_\phi - h_{150}b_\psi] T_4(\gamma_2, \gamma_4)}{\pi}, \\
 D_y^{(2)}(x, y) = & -\frac{((d_{110}m + \beta_{110}n)b_z - d_{110}b_\phi - \beta_{110}b_\psi) e^{\lambda y}}{2\pi} \frac{x}{x^2 + y^2} \\
 & + \frac{e^{\lambda y}}{\pi} ((d_{110}m + \beta_{110}n)b_z - d_{110}b_\phi - \beta_{110}b_\psi) T_4(\gamma_2, \gamma_4), \\
 B_y^{(2)}(x, y) = & -\frac{((\beta_{110}m + \gamma_{110}n)b_z - \beta_{110}b_\phi - \gamma_{110}b_\psi) e^{\lambda y}}{2\pi} \frac{x}{x^2 + y^2} \\
 & + \frac{e^{\lambda y}}{\pi} ((\beta_{110}m + \gamma_{110}n)b_z - \beta_{110}b_\phi - \gamma_{110}b_\psi) T_4(\gamma_2, \gamma_4) \tag{16}
 \end{aligned}$$

in which  $T_3(\gamma_1, \gamma_3)$  and  $T_4(\gamma_2, \gamma_4)$  are given in Appendix A. It is worth mentioning that the stress, electric displacement, and magnetic induction field due to generalized moving dislocation, Eq. (16), are Cauchy singular at the dislocation location.

### 3 The integral equations

The formulation given in the previous section is used to construct integral equations for the analysis of multiple interfacial moving cracks in two bonded dissimilar FGME layers. A crack configuration concerning coordinate system  $x, y$  may be described in parametric form as

$$\begin{aligned}
 x_i = & x_{oi} + l_i s, \\
 y_i = & y_{oi} \quad i = 1, 2, \dots, N \quad -1 \leq s \leq 1, \tag{17}
 \end{aligned}$$

where  $(x_{oi}, y_{oi})$  are the coordinates of the cracks centers,  $N$  represents the number of moving cracks, and  $l_i$  is the half-length of the crack. By Continuous distribution of dislocations with unknown density  $B_{kj}(t)$ ,  $k \in \{z, \phi, \psi\}$  on

the infinitesimal segment  $dl_j$  located on the surface of the  $j$ th crack, we obtain the integral equations of the problem. The traction free condition on the surface of cracks results in  $B_{kj}(t)$ .

$$\left\{ \begin{array}{l} -\frac{\tau_0}{c_{44}} \\ -\frac{D_0}{d_{110m} + \beta_{110n}} \\ -\frac{B_0}{\beta_{110m} + \gamma_{110n}} \end{array} \right\} = \sum_{j=1}^N \int_{-1}^1 \left( \left\{ \begin{array}{l} K_{ij}^{11}(s, t) \\ K_{ij}^{21}(s, t) \\ K_{ij}^{31}(s, t) \end{array} \right\} B_{zj}(t) + \left\{ \begin{array}{l} K_{ij}^{12}(s, t) \\ K_{ij}^{22}(s, t) \\ K_{ij}^{32}(s, t) \end{array} \right\} B_{\varphi j}(t) + \left\{ \begin{array}{l} K_{ij}^{13}(s, t) \\ K_{ij}^{23}(s, t) \\ K_{ij}^{33}(s, t) \end{array} \right\} B_{\psi j}(t) \right) l_j dt. \tag{18}$$

The kernels of integral equations (18) are given in Appendix A. To reduce the problem to a system of integral equations, we introduce the following new unknown functions:

$$\begin{aligned} w_j^-(s) - w_j^+(s) &= l_j \int_{-1}^s B_{zj}(t) dt, \\ \varphi_j^-(s) - \varphi_j^+(s) &= l_j \int_{-1}^s B_{\varphi j}(t) dt, \\ \psi_j^-(s) - \psi_j^+(s) &= l_j \int_{-1}^s B_{\psi j}(t) dt, \quad j = 1, 2, \dots, N. \end{aligned} \tag{19}$$

The no-net-dislocation conditions are

$$\int_{-1}^1 B_{kj}(t) dt = 0 \quad k \in \{z, \varphi, \psi\}. \tag{20}$$

We employ the square-root-singular fundamental function, so that

$$B_{kj}(t) = \frac{g_{kj}(t)}{\sqrt{1-t^2}} \quad -1 \leq t \leq 1 \quad k \in \{z, \varphi, \psi\}, \tag{21}$$

where  $g_{kj}(t)$  are bounded at  $t = \pm 1$ . The system of equations (18) and (20) may be solved for the dislocation densities. The stress, electric displacement, and the magnetic induction intensity factors at the crack tips  $+1$  and  $-1$  are defined as

$$\left\{ \begin{array}{l} (K_R^M)_i \\ (K_R^D)_i \\ (K_R^B)_i \end{array} \right\} = \frac{L_i(+1)}{2} \left\{ \begin{array}{l} \left( \begin{array}{l} c_{44} \\ -e_{15} \\ -h_{15} \end{array} \right) g_{zi(+1)} + \left( \begin{array}{l} e_{15} \\ d_{11} \\ \beta_{11} \end{array} \right) g_{\varphi i(+1)} + \left( \begin{array}{l} h_{15} \\ \beta_{11} \\ \gamma_{11} \end{array} \right) g_{\psi i(+1)} \end{array} \right\}. \tag{22}$$

Similarly,

$$\left\{ \begin{array}{l} (K_L^M)_i \\ (K_L^D)_i \\ (K_L^B)_i \end{array} \right\} = -\frac{L_i(-1)}{2} \left\{ \begin{array}{l} \left( \begin{array}{l} c_{44} \\ -e_{15} \\ -h_{15} \end{array} \right) g_{zi(-1)} + \left( \begin{array}{l} e_{15} \\ d_{11} \\ \beta_{11} \end{array} \right) g_{\varphi i(-1)} + \left( \begin{array}{l} h_{15} \\ \beta_{11} \\ \gamma_{11} \end{array} \right) g_{\psi i(-1)} \end{array} \right\}, \quad i = 1, 2, \dots, N. \tag{23}$$

Finally, the integral equations (18) are solved and field intensity factors are calculated by Eqs. (22) and (23).

### 4 Results and discussion

In this section, some numerical calculations are carried out. As a particular case of the problem, the BaTiO<sub>3</sub>-CoFe<sub>2</sub>O<sub>4</sub> composite material with a volume fraction  $V_f = 0.50$  is considered. Their material properties are given in Table 1.

The upper and lower layers are composites made of BaTiO<sub>3</sub> as the inclusion material and CoFe<sub>2</sub>O<sub>4</sub> as the matrix material. Their properties are shown in Table 1 (2013). Using the following linear mixture rule, the material properties of each composite component are given

$$\chi^{(c)} = \chi^{(i)} V_f + \chi^{(m)} (1 - V_f), \tag{24}$$

**Table 1** Material properties for single-phase and the composite

Material constants (2013)	BaTiO <sub>3</sub>	CoFe <sub>2</sub> O <sub>4</sub>	Composite (1:1)
$c_{44}(\times 10^{10}\text{N/m}^2)$	4.3	4.53	4.4
$e_{15}(\text{C/m}^2)$	11.6	NA	5.8
$d_{11}(\times 10^{-10}\text{C/Vm})$	112	0.8	56.4
$h_{15}(\text{N/Am})$	NA	550	275
$\gamma_{11}(\times 10^{-6}\text{Ns}^2/\text{C}^2)$	5	590	297.5
$\rho(\times 10^3\text{kg/m}^3)$	6.02	5.3	5.7
$\beta_{11}(\times 10^{-11}\text{Ns/VC})$			0.5

where superscripts c, i, and m denote the composite, inclusion, and matrix materials, respectively, and  $V_f$  is the volume fraction of the single-phase BaTiO<sub>3</sub>.

The loading combination parameters are introduced to reflect the corresponding loading combination between electric, magnetic, and mechanical loads.

$$\lambda_D = D_0 e_{15} / \tau_0 d_{11}, \quad \lambda_B = B_0 h_{15} / \tau_0 \beta_{11}. \tag{25}$$

It is convenient to adopt dimensionless parameters in the plots so that we define normalized field intensity factors (FIFs) as

$$K_{0M} = \tau_0 \sqrt{l}, \quad K_{0D} = \tau_0 \sqrt{l} d_{11} / e_{15}, \quad K_{0B} = \tau_0 \sqrt{l} \beta_{11} / h_{15}. \tag{26}$$

In the present paper, we consider the case where the layered smart structure is under constant anti-plane mechanical shear stress  $\sigma_{zy} = \tau_0$ , in-plane electrical loading  $D_y = D_0$ , and magnetic loading  $B_0$ . In the sequel, unless otherwise stated, the loading parameters and the dimensions of the layers are, respectively,  $\lambda_D = 1.0$ ,  $\lambda_B = 1.0$ ,  $h_1 = 0.01m$  and  $h_2 = 0.01m$ .

Results were first validated based on those of an infinite homogeneous MEE plane weakened by moving screw dislocation. This problem was studied by [15]. The problem is reduced to the moving magneto-electroelastic screw dislocation solution of [15] by setting  $h_1 \rightarrow \infty$  and  $h_2 \rightarrow \infty$ .

$$\begin{aligned} \sigma_{zy}(x, y) &= \frac{(\alpha_2 e_{150} + \alpha_3 h_{150} - K \tilde{c}_{44}) b_z}{2\pi} \frac{x}{x^2 + (Ky)^2} - \frac{(e_{150} b_\varphi + h_{150} b_\psi)}{2\pi} \frac{x}{x^2 + y^2}, \\ D_y(x, y) &= -\frac{(\alpha_2 d_{110} + \alpha_3 \beta_{110}) b_z - (d_{110} b_\varphi + \beta_{110} b_\psi)}{2\pi} \frac{x}{x^2 + y^2}, \\ B_y(x, y) &= -\frac{(\alpha_2 \beta_{110} + \alpha_3 \gamma_{110}) b_z - (\beta_{110} b_\varphi + \gamma_{110} b_\psi)}{2\pi} \frac{x}{x^2 + y^2}. \end{aligned} \tag{27}$$

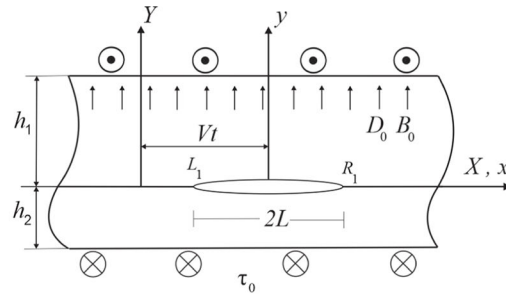
The results are in complete agreement with the results obtained by Tупholme which demonstrate the validity of the dislocation solution. These imply the correctness and accuracy of our results.

### 4.1 Single crack problem

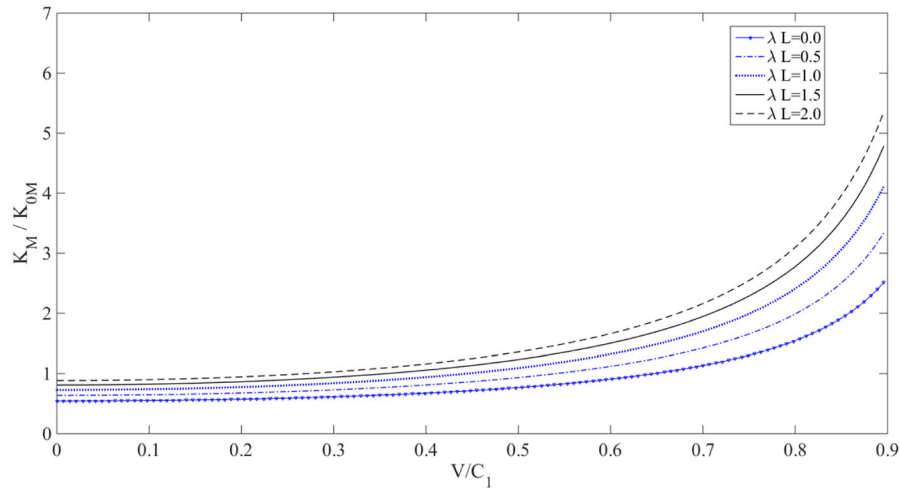
Consider a finite crack with constant length propagating at a constant speed  $V$  along with the interface between two dissimilar functionally graded magneto-electroelastic layers, as shown in Fig. 2a.

Graphical plots of normalized field intensity factors (FIFs) against  $V/C_1$  different values of gradient parameters  $\lambda L$  are presented in Fig. 2. The general feature of these curves is that the FIFs increase with the increase of crack velocity. Significant effects of the material gradient  $\lambda L$  upon stress intensity factors (SIFs) can be observed  $V/C_1 < 0.6$ . However, when the material properties are graded, a significant increase in FIFs is observed with an

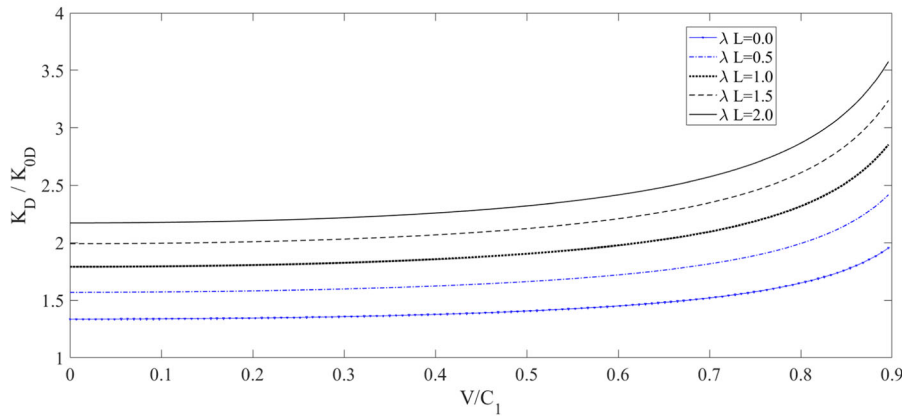




(a) A moving crack at the interface of two dissimilar FGME layers.

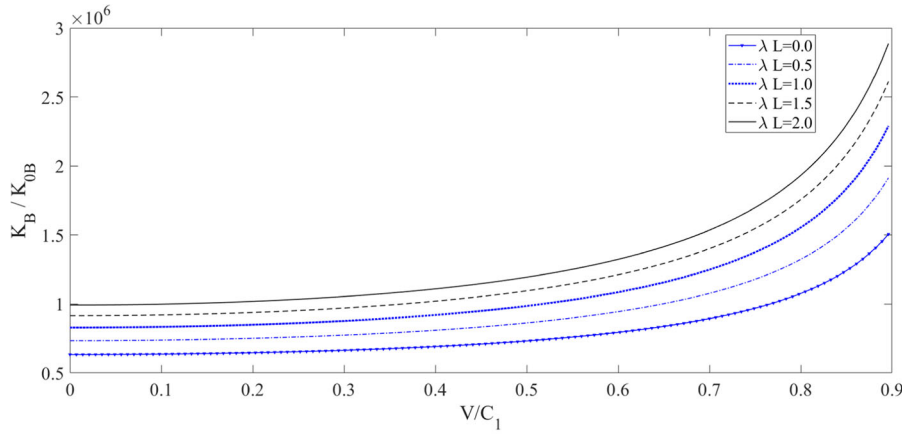


(b) Variation of normalized stress intensity factor versus the crack speed.

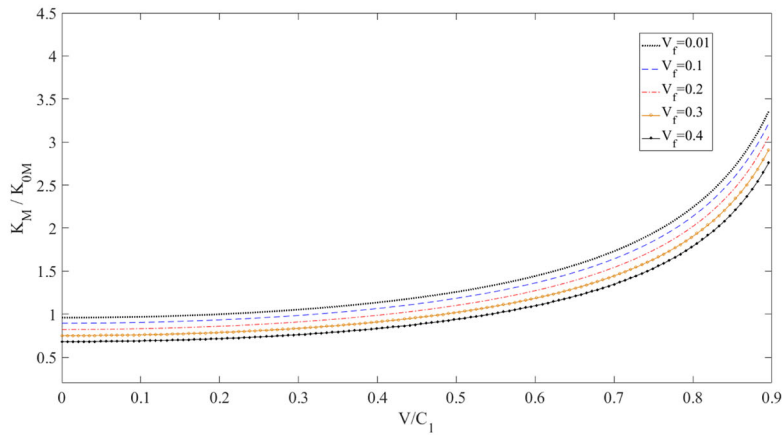


(c) Variation of normalized electric displacement intensity factor versus the crack speed.

**Fig. 2** a A moving crack at the interface of two dissimilar FGME layers. b Variation of normalized stress intensity factor versus the crack speed. c Variation of normalized electric displacement intensity factor versus the crack speed. d Variation of normalized magnetic induction intensity factor versus the crack speed. e Variation of normalized stress intensity factor versus the crack speed for different material volume fractions



(d) Variation of normalized magnetic induction intensity factor versus the crack speed.



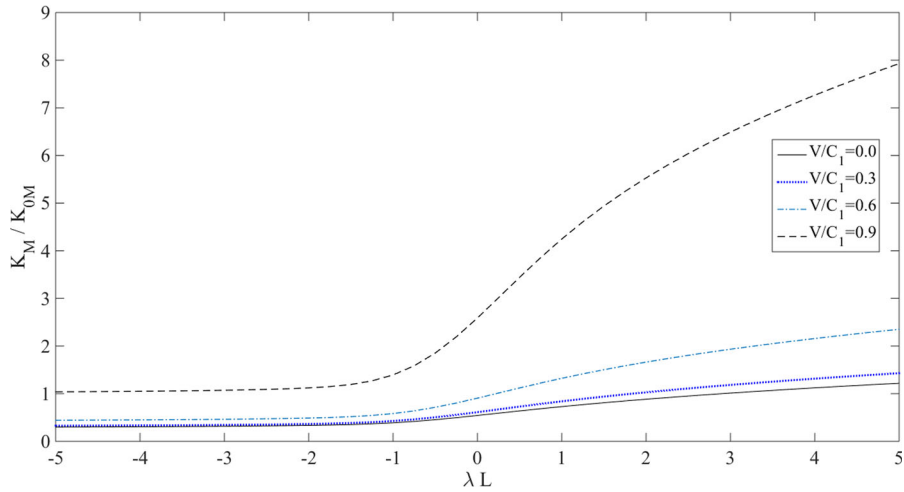
(e) Variation of normalized stress intensity factor versus the crack speed for different material volume fractions.

Fig. 2 continued

increase in crack speed and gradient of the materials. The remarkable difference between different FGM exponents  $\lambda L$  is shown in Fig. 2c and d. Generally speaking, smaller positive values of FGM constants can reduce the FIFs and larger values can lead to larger values of FIFs. To investigate the effect of the composite type on DSIFs, a moving crack at the interface of dissimilar functionally graded MEE layers with different material volume fractions is considered, Fig. 2e. The loading parameters and nonhomogeneous parameter are  $\lambda_D = 1.0$ ,  $\lambda_B = 1.0$  and  $\lambda L = 2.0$ , respectively.

It is shown that, in all composite materials, as the crack velocity increases the SIFs increase. The volume fraction of the single-phase BaTiO<sub>3</sub> has a drastic effect on the dynamic stress intensity factor.

In the next example, the dependency of stress intensity factors of a moving interfacial crack on the FGM exponent is examined. The plots of dimensionless stress intensity factors for different dimensionless crack velocities  $V/C_1$  versus FGM exponent are drawn in Fig. 3. It is observed that stress intensity factors grow rapidly as the FGM exponent increases from the negative to the positive value. A remarkable difference is seen for a higher value of crack velocity.



**Fig. 3** Variation of normalized stress intensity factor versus  $\lambda L$

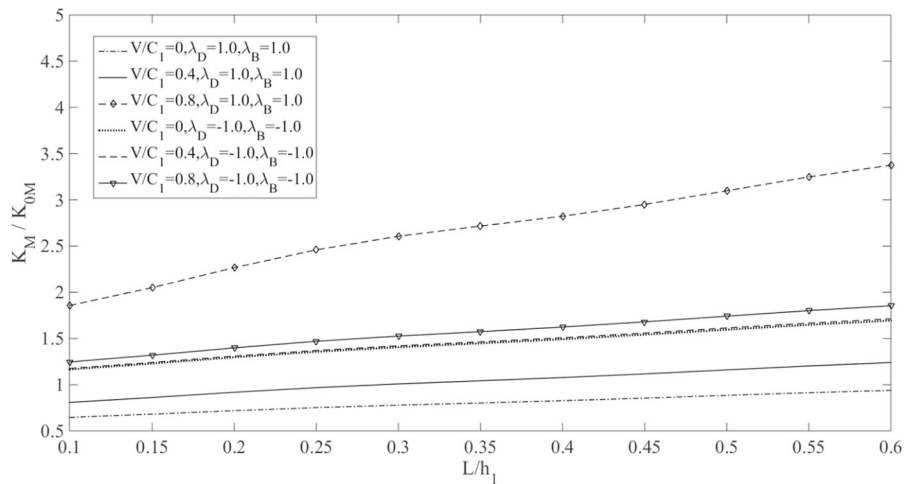


**Fig. 4** Variation of normalized stress intensity factor versus  $L/h_1$

Figure 4 displays the variation of the normalized SIFs against the crack length for different values of normalized crack velocity and loading parameters. It is seen that the SIFs rise with the increase of the crack length. For a very large crack or very thin layer thickness, we obtain the higher values of SIFs.

The SIFs for  $V/C_1 = 0$ , as shown in the figure, correspond to the static solution of an interface crack in two bonded FGME layers under different loading conditions.

We observe that the positive electric or magnetic loading increases the normalized stress intensity factor more than the negative one. Therefore, the sign of electric or magnetic loading could enhance or impede the dielectric crack growth.

#### 4.2 Multiple cracks problem

The formulation may be used for the analysis of multiple moving cracks along with the interface.

**Fig. 5** Two equal-length moving cracks at the interface of two dissimilar FGME layers

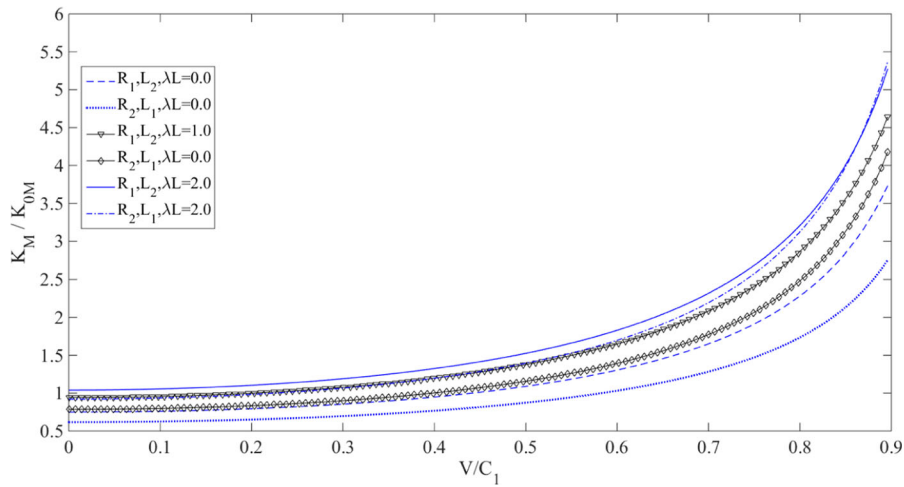
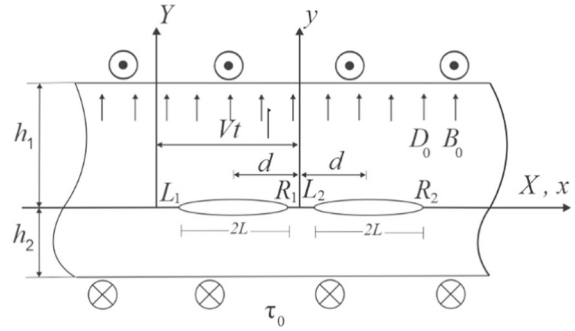


**Fig. 6** Variation of normalized stress intensity factor two interfacial cracks versus  $V/C_1$

The next example deals with the interaction between two identical interfacial moving cracks (Fig. 5). Figure 6, displays the variations of normalized stress intensity factors versus  $V/C_1$  for different ratios of the FGM exponent. It is seen that for large values of FGM exponent, stress intensity factor increases significantly.

Two interfacial equal-length cracks with length  $L = 0.5h$  are shown in Fig. 7. The length of the cracks is fixed while the location of crack centers is changing in the interface. Due to symmetry, as it is expected, the SIFs at  $L_1$  and  $R_1$  are equal to those at  $R_2$  and  $L_2$ , respectively. Also, the interaction of cracks  $d > 1.7L$  is weak and it decays out. It is observed from Fig. 7, the crack velocity has a significant effect on the value of stress intensity factors. Similar phenomena can be observed for other values  $V/C$ .

In the remaining section, more examples are rendered to demonstrate the applicability of the proposed method. Therefore, the study of the interaction between three cracks is taken up, Fig. 8. We observe that interaction between cracks enhances the SIFs of crack  $L_2R_2$  and experiences much larger stress intensity factors. In contrast, crack tips  $L_1$  and  $R_3$  experience smaller SIF than the other tips. It can be seen from Fig. 9 that the stress intensity factors increase as the FG exponent increases.

The model of interfacial unequal cracks is of more practical significance than the widely studied model of equal cracks because actual interfacial cracks are always unequal. As the last example, the study of the interaction between three unequal-length cracks is taken up, Fig. 10.

In comparison with the previous example, we observe that interaction between cracks enhances the SIFs of crack  $L_2R_2$ , which is larger than the other cracks. The SIFs are the lowest at crack tips  $L_1$  and  $R_3$ , which is the farthest crack tip from the other crack tips.

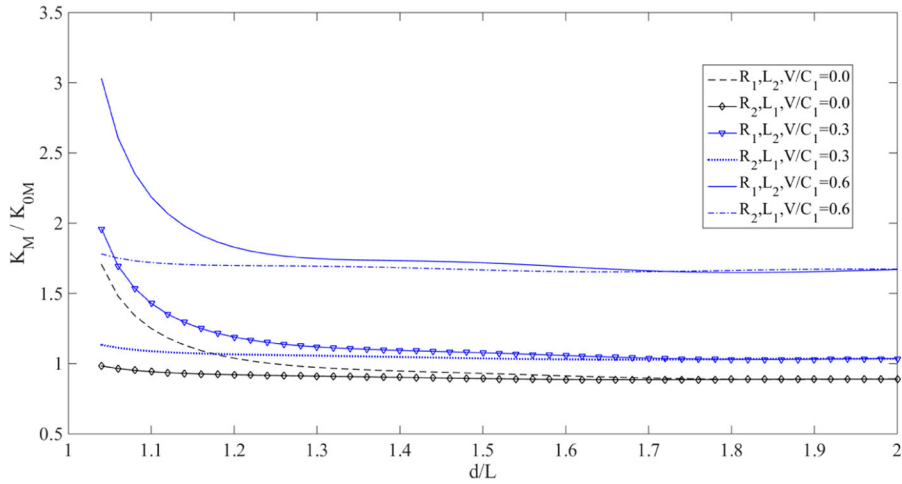


Fig. 7 Variation of normalized stress intensity factor of two interfacial cracks versus  $d/L$

Fig. 8 Three equal-length moving cracks at the interface of two dissimilar FGME layers

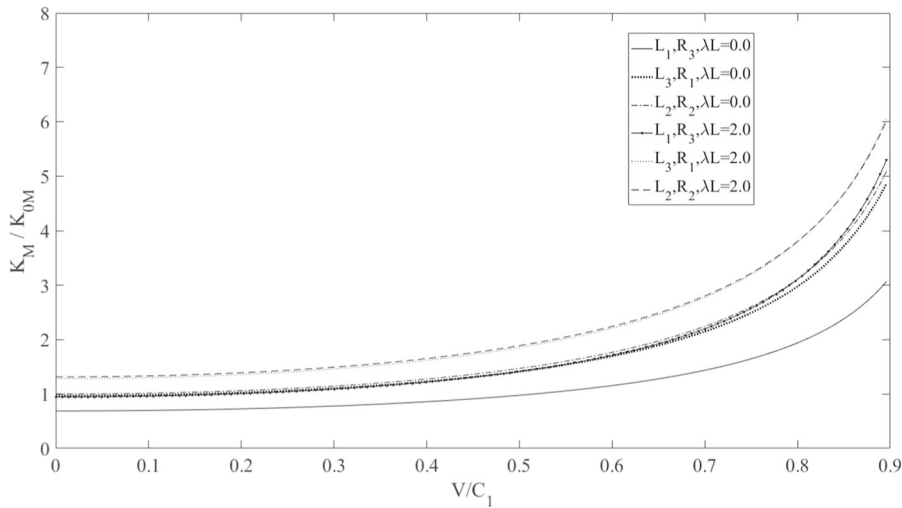
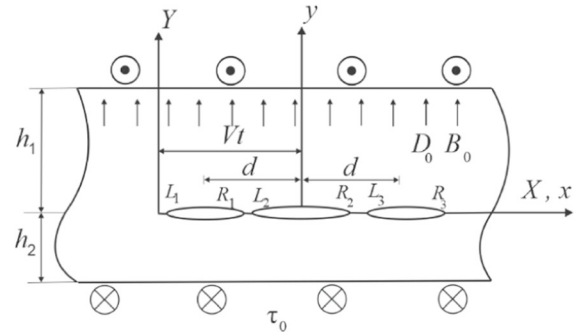
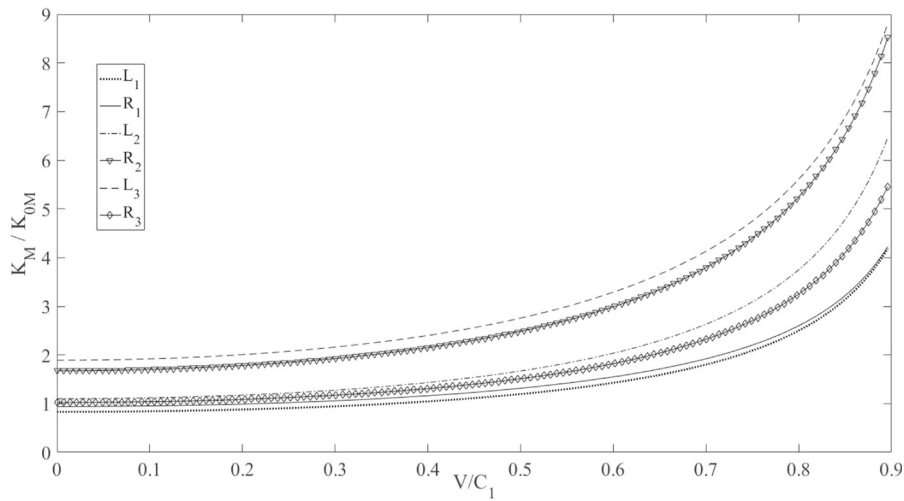
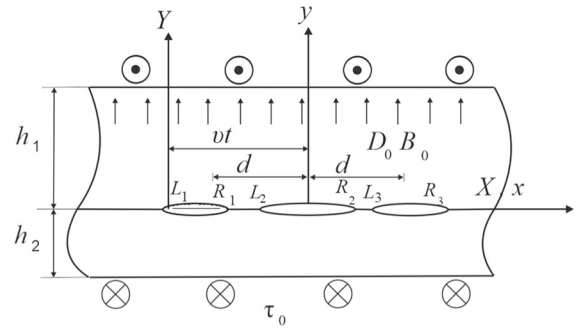


Fig. 9 Variation of normalized stress intensity factor three interfacial cracks versus  $V/C_1$

**Fig. 10** Three unequal-length moving cracks at the interface of two dissimilar FGMEEL layers



**Fig. 11** Variation of normalized stress intensity factor three unequal interfacial moving cracks versus  $V/C_1$

### 5 Conclusions

The dynamic crack problem of moving crack at the interface of two dissimilar functionally graded magnetoelastoelectroelastic layers is studied. The exponential Fourier transform method and distributed dislocation technique are used to construct the singular integral equations with Cauchy type kernel, which is further solved numerically. A generalized dislocation is obtained, which can be used as the fundamental solution for solving multiple interfacial moving cracks problems in two dissimilar nonhomogeneous magnetoelastoelectroelastic layers. The formulation is quite useful in analyzing the problem of multiple interfacial moving cracks.

The results are obtained for different values of the nonhomogeneity parameter  $\lambda L$  at the tips of multiple moving cracks and are shown in Figs. 2, 6, and 9. The figures also show another physically expected result, and the field intensity factors depend on the crack velocity and the sign of loading parameters. It can be concluded that the dynamic field intensity factor increases significantly with the increase of crack velocity. Furthermore, the results are highly affected by the material volume fractions. To study the interaction between cracks, field intensity factors are obtained for some examples. The interaction of multiple moving cracks decreases when the distance between the cracks increases.

**Appendix A**

The coefficients of Eq. (14) are

$$\begin{aligned}
 A_2^{(2)}(\omega) &= \frac{b_z}{P\hat{R} - \hat{P}}(\pi\delta(\omega) - i/\omega), \\
 B_2^{(2)}(\omega) &= \frac{mb_z - b_\varphi}{\hat{Q} - QR}(\pi\delta(\omega) - i/\omega), \\
 C_2^{(2)}(\omega) &= \frac{nb_z - b_\psi}{\hat{Q} - QR}(\pi\delta(\omega) - i/\omega), \\
 A_1^{(2)}(\omega) &= -e^{-2\gamma_3 h_2} \frac{\lambda - \gamma_3}{\lambda + \gamma_3} \frac{b_z}{P\hat{R} - \hat{P}}(\pi\delta(\omega) - i/\omega), \\
 B_1^{(2)}(\omega) &= -e^{-2\gamma_4 h_2} \frac{\lambda - \gamma_4}{\lambda + \gamma_4} \frac{mb_z - b_\varphi}{\hat{Q} - QR}(\pi\delta(\omega) - i/\omega), \\
 C_1^{(2)}(\omega) &= -e^{-2\gamma_4 h_2} \frac{\lambda - \gamma_4}{\lambda + \gamma_4} \frac{nb_z - b_\psi}{\hat{Q} - QR}(\pi\delta(\omega) - i/\omega).
 \end{aligned} \tag{A-1}$$

In the above equations

$$P = 1 - e^{-2\gamma_1 h_1} \frac{\beta + \gamma_1}{\beta - \gamma_1}, \quad \hat{P} = 1 - e^{-2\gamma_3 h_2} \frac{\lambda - \gamma_3}{\lambda + \gamma_3}, \tag{A-2}$$

$$Q = 1 - e^{-2\gamma_2 h_1} \frac{\beta + \gamma_2}{\beta - \gamma_2}, \quad \hat{Q} = 1 - e^{-2\gamma_4 h_2} \frac{\lambda - \gamma_4}{\lambda + \gamma_4}, \tag{A-3}$$

$$R = \frac{(\lambda - \gamma_4)(1 - e^{-2\gamma_4 h_2})}{(\beta + \gamma_2)(1 - e^{-2\gamma_2 h_1})}, \quad \hat{R} = \frac{(\lambda - \gamma_3)(1 - e^{-2\gamma_3 h_2})}{(\beta + \gamma_1)(1 - e^{-2\gamma_1 h_1})}, \tag{A-4}$$

the following functions are used in the field components.

$$T_1(\gamma_1, \gamma_3) = \int_0^{+\infty} (e^{\gamma_3 y} - e^{-\gamma_3(y+2h_2)}) \frac{\lambda - \gamma_3}{\omega(P\hat{R} - \hat{P})} \sin \omega x \, d\omega, \tag{A-5}$$

$$T_2(\gamma_2, \gamma_4) = \int_0^{+\infty} (e^{\gamma_4 y} - e^{-2\gamma_4 h_2} e^{-\gamma_4 y}) \frac{\lambda - \gamma_4}{\omega(\hat{Q} - QR)} \sin \omega x \, d\omega, \tag{A-6}$$

$$T_3(\gamma_1, \gamma_3) = \int_0^{+\infty} \left[ (e^{\gamma_3 y} - e^{-\gamma_3(y+2h_2)}) \frac{\lambda - \gamma_3}{\omega(P\hat{R} - \hat{P})} - \frac{K}{2} e^{K\omega y} \right] \sin \omega x \, d\omega, \tag{A-7}$$

$$T_4(\gamma_2, \gamma_4) = \int_0^{+\infty} \left( (e^{\gamma_4 y} - e^{-\gamma_4(y+2h_2)}) \frac{\lambda - \gamma_4}{\omega(\hat{Q} - QR)} + \frac{e^{\omega y}}{2} \right) \sin \omega x \, d\omega, \tag{A-8}$$

The kernels of singular integral equations (18) are:

$$\begin{aligned}
 K_{ij}^{11}(s, t) &= -\frac{K e^{\lambda(y_i - y_j)}}{2\pi} \frac{x_i - x_j}{(x_i - x_j)^2 + [K(y_i - y_j)]^2} + \frac{[(e_{150}m + h_{150}n)]e^{\lambda(y_i - y_j)}}{2\pi \tilde{c}_{44}} \frac{x_i - x_j}{(x_i - x_j)^2 + (y_i - y_j)^2}, \\
 &\quad - \int_0^{+\infty} \left[ \frac{(\lambda - \gamma_3)(e^{\gamma_3(y_i - y_j)} - e^{-\gamma_3((y_i - y_j) + 2h_2)})}{\omega(P\hat{R} - \hat{P})} - \frac{K}{2} e^{k\omega(y_i - y_j)} \right] \sin \omega(x_i - x_j) \, d\omega,
 \end{aligned}$$

$$\begin{aligned}
& -\frac{(e_{150m} + h_{150n})e^{\lambda(y_i - y_j)}}{\pi \tilde{c}_{44}} \int_0^{+\infty} \left[ \frac{(\lambda - \gamma_4)(e^{\gamma_4(y_i - y_j)} - e^{-\gamma_4((y_i - y_j) + 2h_2)})}{\omega(\hat{Q} - QR)} + \frac{1}{2} e^{\omega(y_i - y_j)} \right] \\
& \quad \times \sin \omega(x_i - x_j) d\omega, \\
K_{ij}^{12}(s, t) &= -\frac{e_{150} e^{\lambda(y_i - y_j)}}{2\pi \tilde{c}_{44}} \frac{x_i - x_j}{(x_i - x_j)^2 + (y_i - y_j)^2} + \frac{e_{150} e^{\lambda(y_i - y_j)}}{\pi \tilde{c}_{44}}, \\
& \quad \times \int_0^{+\infty} \left[ \frac{(\lambda - \gamma_4)(e^{\gamma_4(y_i - y_j)} - e^{-\gamma_4((y_i - y_j) + 2h_2)})}{\omega(\hat{Q} - QR)} + \frac{1}{2} e^{\omega(y_i - y_j)} \right] \sin \omega(x_i - x_j) d\omega, \\
K_{ij}^{13}(s, t) &= -\frac{h_{150} e^{\lambda(y_i - y_j)}}{2\pi \tilde{c}_{44}} \frac{x_i - x_j}{(x_i - x_j)^2 + (y_i - y_j)^2} + \frac{h_{150} e^{\lambda(y_i - y_j)}}{\pi \tilde{c}_{44}} \\
& \quad \times \int_0^{+\infty} \left[ \frac{(\lambda - \gamma_4)(e^{\gamma_4(y_i - y_j)} - e^{-\gamma_4((y_i - y_j) + 2h_2)})}{\omega(\hat{Q} - QR)} + \frac{e^{\omega(y_i - y_j)}}{2} \right] \sin \omega(x_i - x_j) d\omega, \\
K_{ij}^{21}(s, t) &= \frac{e^{\lambda(y_i - y_j)}}{2\pi} \frac{x_i - x_j}{(x_i - x_j)^2 + (y_i - y_j)^2} + \frac{e^{\lambda(y_i - y_j)}}{\pi} \\
& \quad \times \int_0^{+\infty} \left[ \frac{(\lambda - \gamma_4)(e^{\gamma_4(y_i - y_j)} - e^{-\gamma_4((y_i - y_j) + 2h_2)})}{\omega(\hat{Q} - QR)} + \frac{e^{\omega(y_i - y_j)}}{2} \right] \sin \omega(x_i - x_j) d\omega, \\
K_{ij}^{22}(s, t) &= \frac{d_{110} e^{\lambda(y_i - y_j)}}{2\pi(d_{110m} + \beta_{110n})} \frac{x_i - x_j}{(x_i - x_j)^2 + (y_i - y_j)^2} - \frac{d_{110} e^{\lambda(y_i - y_j)}}{\pi(d_{110m} + \beta_{110n})}, \\
& \quad \times \int_0^{+\infty} \left[ \frac{(\lambda - \gamma_4)(e^{\gamma_4(y_i - y_j)} - e^{-\gamma_4((y_i - y_j) + 2h_2)})}{\omega(\hat{Q} - QR)} + \frac{e^{\omega(y_i - y_j)}}{2} \right] \sin \omega(x_i - x_j) d\omega, \\
K_{ij}^{23}(s, t) &= \frac{\beta_{110} e^{\lambda(y_i - y_j)}}{2\pi(d_{110m} + \beta_{110n})} \frac{x_i - x_j}{(x_i - x_j)^2 + (y_i - y_j)^2} - \frac{\beta_{110} e^{\lambda(y_i - y_j)}}{\pi(d_{110m} + \beta_{110n})}, \\
& \quad \times \int_0^{+\infty} \left[ \frac{(\lambda - \gamma_4)(e^{\gamma_4(y_i - y_j)} - e^{-\gamma_4((y_i - y_j) + 2h_2)})}{\omega(\hat{Q} - QR)} + \frac{e^{\omega(y_i - y_j)}}{2} \right] \sin \omega(x_i - x_j) d\omega, \\
K_{ij}^{31}(s, t) &= \frac{e^{\lambda(y_i - y_j)}}{2\pi} \frac{x_i - x_j}{(x_i - x_j)^2 + (y_i - y_j)^2} + \frac{e^{\lambda(y_i - y_j)}}{\pi}, \\
& \quad \times \int_0^{+\infty} \left[ \frac{(\lambda - \gamma_4)(e^{\gamma_4(y_i - y_j)} - e^{-\gamma_4((y_i - y_j) + 2h_2)})}{\omega(\hat{Q} - QR)} + \frac{e^{\omega(y_i - y_j)}}{2} \right] \sin \omega(x_i - x_j) d\omega, \\
K_{ij}^{32}(s, t) &= \frac{\beta_{110} e^{\lambda(y_i - y_j)}}{2\pi(\beta_{110m} + \gamma_{110n})} \frac{x_i - x_j}{(x_i - x_j)^2 + (y_i - y_j)^2} - \frac{\beta_{110} e^{\lambda(y_i - y_j)}}{\pi(\beta_{110m} + \gamma_{110n})}, \\
& \quad \times \int_0^{+\infty} \left[ \frac{(\lambda - \gamma_4)(e^{\gamma_4(y_i - y_j)} - e^{-\gamma_4((y_i - y_j) + 2h_2)})}{\omega(\hat{Q} - QR)} + \frac{e^{\omega(y_i - y_j)}}{2} \right] \sin \omega(x_i - x_j) d\omega, \\
K_{ij}^{33}(s, t) &= \frac{\gamma_{110} e^{\lambda(y_i - y_j)}}{2\pi(\beta_{110m} + \gamma_{110n})} \frac{x_i - x_j}{(x_i - x_j)^2 + (y_i - y_j)^2} - \frac{\gamma_{110} e^{\lambda(y_i - y_j)}}{\pi(\beta_{110m} + \gamma_{110n})},
\end{aligned}$$



$$\times \int_0^{+\infty} \left[ \frac{(\lambda - \gamma_4)(e^{\gamma_4(y_i - y_j)} - e^{-\gamma_4((y_i - y_j) + 2h_2)})}{\omega(\hat{Q} - QR)} + \frac{e^{\omega(y_i - y_j)}}{2} \right] \sin \omega(x_i - x_j) d\omega. \quad (\text{A-9})$$

## References

1. Chen Z, Yu S (1997) Anti-plane Yoffe crack problem in piezoelectric materials. *Int J Fract* 84:L41–L45
2. Kwon JH, Lee KY (2000) Moving interfacial crack between piezoelectric ceramic and elastic layers. *Eur J Mech A Solids* 19:979–987
3. Wang X, Zhong Z, Wu FL (2003) A moving conducting crack at the interface of two dissimilar piezoelectric materials. *Int J Solids Struct* 40:2381–2399
4. Bagheri R, Ayatollahi M, Mousavi SM (2015) Analytical solution of multiple moving cracks in functionally graded piezoelectric strip. *Appl Math Mech* 36:777–792
5. Gao CF, Pin T, Yi Z (2003) Interfacial crack problems in magneto-electro elastic solids. *Int J Eng Sci* 41:2105–2121
6. Gao CF, Noda N (2004) Thermal-induced interfacial cracking of magneto-electroelastic materials. *Int J Eng Sci* 42:1347–1360
7. Hu K, Li G (2005) Constant moving crack in a magneto-electroelastic material under anti-plane shear loading. *Int J Solids Struct* 42:2823–2835
8. Hu KQ, Kang YL, Li GL (2006) Moving crack at the interface between two dissimilar magneto-electroelastic materials. *Acta Mech* 182:1–16
9. Zhong XC, Li XF (2006) A finite length crack propagating along the interface of two dissimilar magneto-electroelastic materials. *Int J Eng Sci* 44:1394–1407
10. Zhao SX, Lee KY (2007) Moving interfacial crack between two dissimilar soft ferromagnetic materials in uniform magnetic field. *J Mech Sci Tech* 21:745–754
11. Hu KQ, Kang YL, Qin QH (2007) A moving crack in a rectangular magneto-electroelastic body. *Eng Fract Mech* 74:751–770
12. Feng WJ, Pan E (2008) Dynamic fracture behavior of an internal interfacial crack between two dissimilar magneto-electro-elastic plates. *Eng Fract Mech* 75:1468–1487
13. Tupholme GE (2009) Moving antiplane shear crack in transversely isotropic magneto-electroelastic media. *Acta Mech* 202:153–162
14. Shin JW, Lee YS (2010) A moving interface crack between two dissimilar functionally graded piezoelectric layers under electromechanical loading. *Int J Solids Struct* 47:2706–2713
15. Tupholme GE (2012) Magneto-electroelastic media containing a row of moving shear cracks. *Mech Res Commun* 45:48–53
16. Fu J, Hu K, Chen Z, Qian L (2013) A moving crack propagating in a functionally graded magneto-electroelastic strip under different crack face conditions. *Theor Appl Fract Mech* 66:16–25
17. Hu K, Chen Z (2013) Pre-kinking of a moving crack in a magneto-electroelastic material under in-plane loading. *Int J Solids Struct* 50:2667–2677
18. Hu K, Chen Z (2014) An interface crack moving between magneto-electroelastic and functionally graded elastic layers. *Appl Math Model* 38:910–925
19. Yue Y, Wan Y (2014) Multilayered piezomagnetic/piezoelectric composite with periodic interfacial Yoffe-type cracks under magnetic or electric field. *Acta Mech* 225:2133–2150
20. Hu K, Chen Z, Fu J (2015) Moving Dugdale crack along the interface of two dissimilar magneto-electroelastic materials. *Acta Mech* 226:2065–2076
21. Xia X, Zhong Z (2015) A mode III moving interfacial crack based on strip magneto-electric polarization saturation model. *Smart Mater Struct* 24:1–15
22. Bagheri R, Ayatollahi M, Mousavi SM (2015) Stress analysis of a functionally graded magneto-electro-elastic strip with multiple moving cracks. *Math Mech Solids* 22:304–323
23. Ma P, Su RKL, Feng WJ (2017) Moving crack with a contact zone at interface of magneto-electroelastic biomaterial. *Eng Fract Mech* 181:143–160
24. Ayatollahi M, Mahmoudi Monfared M, Nourazar M (2017) Analysis of multiple moving mode-III cracks in a functionally graded magneto-electroelastic half-plane. *J Intell Mater Syst Struct* 28:2823–2834
25. Bagheri RM, Noroozi M (2018) The linear steady state analysis of multiple moving cracks in a piezoelectric half-plane under in-plane electro-elastic loading. *Theor Appl Fract Mech* 96:334–350